Constraints on Dynamical Dark Energy Models from the Abundance of Massive Galaxies at High Redshifts

Menci N, Grazian A, Castellano M, P Santini,, E. Giallongo, A. Lamastra, Fortuni F, Fontana A, Merlin E, Wang T, et al.

Constraints on Dynamical Dark Energy Models from the Abundance of Massive Galaxies at High Redshifts

12 authors, including:

Andrea Grazian
National Institute of Astrophysics
265 PUBLICATIONS   11,121 CITATIONS

SEE PROFILE

Marco Castellano
National Institute of Astrophysics
182 PUBLICATIONS   5,436 CITATIONS

SEE PROFILE

Paola Santini
National Institute of Astrophysics
199 PUBLICATIONS   8,062 CITATIONS

SEE PROFILE

A. Lamastra
National Institute of Astrophysics
66 PUBLICATIONS   1,316 CITATIONS

SEE PROFILE

Some of the authors of this publication are also working on these related projects:

Project   The New Universe - Le Nouvel Univers View project

Project   CANDELS View project

Constraints on Dynamical Dark Energy Models from the Abundance of Massive Galaxies at High Redshifts

N. Menci[1], A. Grazian[2], M. Castellano[1], P. Santini[1], E. Giallongo[1], A. Lamastra[1], F. Fortuni[1], A. Fontana[1], E. Merlin[1], T. Wang[3], D. Elbaz[4], N.G. Sanchez[5].

[1]*INAF - Osservatorio Astronomico di Roma, via Frascati 33, I-00078 Monteporzio, Italy*
[2]*INAF–Osservatorio Astronomico di Padova, Vicolo dell'Osservatorio 5, I-35122, Padova, Italy*
[3]*National Astronomical Observatory of Japan, Mitaka, Tokyo, Japan*
[4]*AIM, CEA, CNRS, Universite Paris-Saclay, Universite Paris Diderot, Sorbonne Paris Cite, Gif-sur-Yvette, France*
[5]*LERMA, CNRS UMR 8112, 61, Observatoire de Paris PSL, Sorbonne Universités, UPMC Univ. Paris 6, 61 Avenue de l'Observatoire, F-75014 Paris, France*

Abstract

We compare the maximal abundance of massive systems predicted in different dynamical dark energy (DDE) models at high redshifts $z \approx 4 - 7$ with the measured abundance of the most massive galaxies observed to be already in place at such redshifts. The aim is to derive constraints for the evolution of the dark energy equation of state parameter w which are complementary to existing probes. We adopt the standard parametrization for the DDE evolution in terms of the local value w_0 and of the look-back time derivative w_a of the equation of state. We derive robust constraints on combinations of (w_0, w_a) in the different DDE models by using three different and independent probes: (i) First, we compare the observed stellar mass function of massive objects at $z \geq 6$ derived from the CANDELS survey with the halo mass function predicted in the different DDE models. (ii) Second, we consider the estimated volume density of massive halos derived from the observation of massive, star-forming galaxies detected in the submillimeter range at $z \approx 4$, and compare it with the predicted halo abundance at the same redshift in the different DDE models. (iii) We consider the most massive system (estimated gas mass exceeding $3 \cdot 10^{11} M_\odot$) observed to be in place at $z \approx 7$, a far-infrared-luminous object recently detected in the South Pole Telescope (SPT) survey. We derive the probability for such an object to be detected in the area covered by SPT for different DDE models, and we compute the corresponding exclusion plots in the $(w_0 - w_a)$ plane. Finally, we show that the combination of our results from the three above probes *excludes a sizable fraction* of the DDE parameter space $w_a \gtrsim -3/4 - (w_0 + 3/2)$ presently allowed (or even favored) by existing probes.

Subject headings: cosmology: cosmological parameters – galaxies: abundances – galaxies: formation

1. Introduction

The current theory of structure formation envisages all cosmic structures to form from the collapse and the growth of initially tiny density perturbations of dark matter (DM) density field in a Universe characterized by an accelerated expansion. Such an acceleration indicates that dominant component of the cosmic fluid must be constituted by some form of dark energy (DE), with equation-of-state parameter $w \equiv p/\rho \leq -1/3$. Although the nature of such a component remains unknown, the simplest model assumes DE to be con-

nected with the vacuum energy, the so-called cosmological constant, with equation-of-state parameter $w = -1$. When coupled with the assumption that DM is constituted by non-relativistic particles at decoupling, such a scenario leads to the ΛCDM standard cosmological model.

While measurements of the Cosmic Microwave Background (CMB) have provided a first, strong confirmation of such a scenario, tensions are recently emerging (mostly between measurements related to the early and late universe): these include the inadequacy of the model in providing a perfect fit to the

Planck CMB temperature and polarization angular spectra (see, e.g., Addison et al. 2016), the discrepancy between the combined values of the power spectrum normalization σ_8 and matter density parameter Ω_M derived by Planck with respect to those derived from cosmic shear surveys such as CFHTLenS (Heymans et al. 2012) and KiDS-450 (Hildebrandt et al. 2017), and - most of all - the tension (at more than 3-σ confidence level) in the Hubble constant H_0 between the values derived from Planck and those obtained from local luminosity distance measurements (see Riess 2019 and references therein).

Such tensions have stimulated an extended effort toward the investigation of more complex cosmological models. One of the simplest physical alternatives is constituted by a DE with time-dependent equation of state (dynamical dark energy, DDE). In fact, this kind of scenario constitutes a possible solution to the above mentioned tension between the values of the Hubble constant derived from local indicators and from the CMB (Di Valentino, Melchiorri, Linder, Silk 2017; Pan, Yang, Di Valentino et al. 2019). In addition, a constant equation of state is not expected in physically motivated scenarios in which DE originates from a scalar "quintessence" field ϕ (Peebles, Ratra 1988; Caldwell, Dave, Steinhardt 1998; Sahni, Wang, 2000; Copeland, Sahni, Tsujikawa, 2006; Frieman, Turner, Huterer 2008) evolving in a potential $V(\phi)$. In fact, its pressure $p_\phi = \dot{\phi} - V(\phi)$ and energy density $\rho_\phi = \dot{\phi} + V(\phi)$ lead to a DE with a time-evolving equation of state parameter $w \equiv p_\phi/\rho_\phi$. Parametrizing the evolution of w with the expansion factor a as $w(a) = w_0 + w_a(1 - a)$ (Chevallier and Polarski 2001, Linder 2003) the dynamics of such models can be related to different combinations (w_0, w_a) (see Caldwell and Linder 2005; Barger Guarnaccia, Marfatia 2006; Linder 2006). E.g., "thawing" models (Scherrer 2008; Chiba 2009; Gupta, Rangarajan, Sen 2015) are characterized by w growing with time starting from $w = -1$ in the early universe, while in "freezing" models (Chiba 2006; Scherrer 2006; Sahlen, Liddle, Parkinson 2007) w decreases with a approaching a cosmological constant value $w = -1$.

Present observational constraints on the DDE parameter space $w_0 - w_a$ (see, e.g., Zhai et al. 2017) provide contrasting results. On the one hand, results coming from the CMB power spectrum (Planck collaboration, Ade et al. 2016) and weak lensing tomography (Massey et al. 2007, Amara and Refregier 2007; see Refregier 2003 for a review) - although leaving

relatively large volume of the DDE parameter space $w_0 - w_a$ - disfavor combinations with $w_0 \lesssim -1.5$ and positive values of $w_a \gtrsim 0.7$ (especially when combined with constraints from baryonic acoustic oscillations and from type-Ia Supernovae, see Ade et al. 2016; Scolnic 2018; di Valentino et al. 2017 and references therein), as well as most of the combinations $w_0 \gtrsim -1$ and $w_a \gtrsim 0.5$. On the other hand, the recent determination of the Hubble diagram of quasars in the range $0.5 \leq z \leq 5.5$ (Risaliti and Lusso 2019) favors large values $w_a \gtrsim 0$ with negative values of $w_0 < -1$, with a deviation from the ΛCDM model emerging with a statistical significance of 4σ. This measurement is based on quasar distances estimated from the ratio between their X-ray and ultraviolet emission. Although it strongly relies on the assumed invariance with redshift of the X-ray-to-ultraviolet ratio, the excellent agreement with the Hubble diagram derived from type-Ia Supernovae in the overlapping range $0.5 \leq z \leq 1.5$ and the evidence of non-evolving UV and X-ray spectral properties strongly argue for the reliability of such results.

In such a context, a further, independent probe for the nature and evolution of DE is constituted by the evolution of the galaxy population over cosmic time. In fact, the inverse dependence of the amplitude of initial density perturbation on the mass scale (measured from fluctuations of the CMB, see, e.g., Tegmark and Zaldarriaga 2002, 2009; Aghanim et al. 2019) implies that the formation of galactic DM halos proceeds bottom-up. Although the physics of baryons assembling into the DM halos constitutes a complex issue, a solid consequence of the above scenario is that - in any specific adopted cosmological model - large-mass DM haloes must become progressively rarer with increasing redshift. Thus, viable cosmological models must allow for an evolution of the initial density perturbations fast enough to match the abundance of massive galaxies observed to be in place early on in history of the Universe. Indeed, several observations concerning massive galaxies at high redshifts are already challenging the canonical ΛCDM cosmological model. E.g., several authors (see, e.g., Hildebrandt et al. 2009; Lee et al. 2012; Caputi et al. 2015; Finkelstein et al. 2015; Merlin et al. 2019; see also Wang et al. 2019) have enlightened the tension between the expected evolution of the DM halo mass function and the observed galaxy luminosity and mass functions at $z \gtrsim 4$. While the present understanding of the baryonic processes leading to gas condensation and to star formation in

DM halos struggles in describing the rapid evolution of the star formation needed to match the observed abundance of massive galaxies (see Steinhardt et al. 2016), an enhanced efficiency in converting baryons into stars at high redshifts could still allow for consistency between the ΛCDM predictions and the observed number density of luminous, massive galaxies (Behroozi et al. 2013; Behroozi and Silk 2015; Finkelstein et al. 2015; Sun and Furlanetto 2016; Moster et al. 2018, Behroozi and Silk 2018).

The above degeneracy between baryonic effects and cosmology in determining the expected abundance of luminous galaxies can be bypassed by noticing that the ratio of galaxy baryonic components (stellar mass or gas mass) to DM halo mass has an absolute maximum at the cosmic baryon fraction $f_b \approx 0.16$ (Aghanim et al., Planck Collaboration, 2018). In fact, the observed abundance of galaxies with large mass in the baryonic component M_b places a lower limit on the abundance of DM haloes with masses $M \geq M_b/f_b \approx 6.3\,M_b$. Such a constrain can be used to rule out cosmological models which do not allow for a sufficiently rapid growth of galactic DM halos. In fact, an observed abundance $\phi_{obs}(M_b, z)$ would rule out any cosmological models predicting a number density of DM haloes $\phi(M \geq M_b/f_b, z) \leq \phi_{obs}(M_b, z)$ independently of the details of the complex baryon physics involved in the galaxy formation process.

In this paper we apply such a probe to cosmological models based on dynamical dark energy (DDE). We compare the maximal abundance of massive galaxies predicted in different DDE models at high redshifts with the measured abundance of the most massive systems observed to be already in place at the same redshifts.

The plan of the paper is as follows:
• in Sect. 2 we present the method adopted to derive the halo mass function in different DDE models, and how we compute the basic quantities that we will compare with observational data.
• Such a comparison is performed in Sect. 3 for three different observations concerning the abundance of massive objects at high redshift: we first compare the observed stellar mass function of massive objects at $z \geq 6$ derived from the CANDELS survey with the halo mass function predicted in different DDE models (Sect. 3.1), deriving exclusion plots in the DDE parameter space $w_0 - w_a$. In Sect. 3.2 we perform a comparison with the estimated volume density of massive halos derived from the observation of massive, star-

forming galaxies detected in the submillimeter at $z \gtrsim 4$ (Wang et al. 2019), which are expected to reside in the most massive DM haloes at their redshift. Finally, in sect. 3.3 we consider the most massive object (estimated gas mass exceeding $3 \cdot 10^{11}\,M_\odot$) in place at $z \approx 7$ recently detected in the SPT survey, and we derive (adopting the most conservative assumptions for the baryon-to-DM ratio) the probability for such a massive object to be present in the area covered by SPT for different DDE models for different combinations (w_0, w_a). The constraints derived from the combination of the above observations are shown in Sect. 3.4.
• The final Sect. 4 is devoted to discussion and conclusions.

2. Method

To compute the expected abundance of DM haloes in different DDE we adopt the canonical Press and Schechter approach, which relates the number of halos of mass M at redshift z to the overdense regions of the linear density field with density contrast δ over a background average density $\bar{\rho}$. Successful models predict the halo mass function ϕ (i.e., the number of virialized DM haloes with mass in the range $M - M + dM$ per unit volume) to take the form

$$\phi(M) = \frac{dN}{dM} = \frac{\bar{\rho}}{M^2} \frac{d\ln\nu}{d\,\ln M}\,f(\nu) \qquad (1)$$

Here $\nu = \delta_c/\sigma(M, z)$ where δ_c corresponds to the critical linear overdensity (equal to 1.69 in the ΛCDM scenario) and $\sigma(M, z)$ is the variance of the linear density field smoothed on the scale $R = [3M/4\pi\bar{\rho}]^{1/3}$, and evolving with time according to the linear growth factor $D(z)$ of density perturbations. The function $f(\nu)$ is universal to the changes in redshift and cosmology. In the original Press-Schechter theory (Press and Schechter 1974) and in excursion set theory (Bond et al. 1991) the function f takes the form $f_{PS} = (\sqrt{2/\pi})^{1/2}\nu\,exp(-\nu^2/2)$ appropriate for spherical collapse. More recent approaches (Sheth and Tormen 1999, Jenkins et al. 2001; Warren et al. 2006; Tinker et al. 2008) provided more accurate forms that have been extensively tested against N-body simulations. Here we adopt the form given by Sheth and Tormen (1999):

$$f(\nu) = 2\,A\left(\frac{1}{\nu'^{2q}} + 1\right)\frac{\nu'^2}{2\,\pi}e^{-\nu'^2/2}. \qquad (2)$$

with $\nu' = \sqrt{a}\nu$, $a = 0.71$, $q = 0.3$. The normalization factor (ensuring that integral of $f(\nu)$ gives

unity) is $A = 0.32$. Corresponding theoretical advances (see, e.g., Sheth et al. 2001, Maggiore and Riotto 2010, Corasaniti and Achitouv, 2011a; Achitouv and Corasaniti 2012) have enlightened the physical meaning of the coefficients and of their numerical value, and showed that they account not only for the non-spherical form of the collapse, but also for more complex aspects of the underlying dynamics. Starting from Sheth and Tormen (2001) the above expression has been extensively tested against N-body simulations for a variety of cosmologies, which showed that such a form can be considered universal with cosmology to within a few per cent (Corasaniti and Achitouv, 2011b; Despali, Giocoli, Angulo et al. 2016). As for the threshold δ_c, we notice that in principle this depends weakly on cosmology. Here we shall adopt the conservative value $\delta_c = 1.65$ for all DDE models. This constitutes a lower bound for the possible values taken in different DDE cosmologies (Mainini, Maccio, Bonometto, Klypin 2003; Pace, Waizmann, Bartelmann 2010) thus maximizing the predicted abundance of massive DM halos.

The mass function dN/dM (eq. 1) allows us to compute the expected number of galaxies in a given region of mass and redshift over a given fraction of the sky, f_{sky} as

$$N = f_{sky} \int dz \frac{dV}{dz} \int dM \frac{dN}{dM} \qquad (3)$$

where the z and M integrals are over the region of the (M, z) plane being considered.

The above expressions depends on the assumed power spectrum of perturbations (determining the dependence of σ on the mass M) and on cosmology, which affects the volume element dV/dz and the growth factor of perturbations $D(z)$.

For the first we adopt the CDM form (Bardeen et al. 1986), which has long been known to provide an excellent match to a wide set of observational data (see Tegmark and Zaldarriaga 2002; Tegmark and Zaldarriaga 2009; Hlozek et al. 2012). The dependence on cosmology (and in particular on the DE equation of state) constitutes our main focus here. In the present paper, we follow the approach adopted in Lamastra et al. (2012), to which we refer for further details. Here we summarize the key points.

We assume a spatially flat, homogeneous and isotropic universe filled by non-relativistic matter plus a dark energy component. For our analysis, we use the Chevallier-Polarski-Linder parametrization (Cheval-

lier and Polarski 2001, Linder 2003) to describe the evolution in terms of the scale factor a (normalized to unity at the present cosmic time):

$$w(a) = w_0 + w_a(1 - a) = w_0 + w_a \frac{z}{1 + z} \qquad (4)$$

where the parameter w_0 represents the value of w at the present epoch, while w_a corresponds to its lookback time variation $w_a = -dw/da$. In the above parametrization, the standard ΛCDM cosmology corresponds to $w_0 = -1$ and $w_a = 0$. Using this parametrization the cosmic expansion described by $H = \dot{a}/a$ given by

$$E(z) \equiv H/H_0 = [\Omega_M a^{-3} + \Omega_\Lambda a^{-3(1+w_0+w_a)} e^{3w_a(a-1)}]^{1/2}. \qquad (5)$$

The above equation also yields the line-of-sight comoving distance corresponding to a distant object at redshift z in any DE model:

$$\chi(z) = \frac{c}{H_0} \int_0^z \frac{dz'}{E(z')}. \qquad (6)$$

This enters the expression for the luminosity and angular distances, and for the volume element dV/dz (see, e.g., Weinberg 1972). In the following we will indicate as V_{w_0,w_a} the cosmic volume computed for DDE cosmologies, while V_Λ is the same quantity computed in the case $w_0 = -1$ and $w_a = 0$ (cosmological constant).

As for the growth factor, its expression in the ΛCDM case is given by Carroll, Press, Turner (1992) in the form :

$$\delta(a) = \frac{5\Omega_M}{2a} \frac{da}{d\tau} \int_0^a \left(\frac{da'}{d\tau}\right)^{-3} da' \qquad (7)$$

where $\tau = H_0 t$. For the DDE models we use the parametrization to the solution given in Linder (2005):

$$\frac{\delta(a)}{a} = exp\left(\int_0^a [\Omega(a)^\gamma - 1]dlna\right) \qquad (8)$$

where $\Omega(a) = \Omega_M a^{-3}/(H(a)/H_0)^2$, and γ is the growth index, given by the fitting formula (Linder 2005):

$$\gamma = 0.55 + 0.05(1 + w(z = 1)) \quad w(z = 1) \geq -1$$
$$\gamma = 0.55 + 0.02(1 + w(z = 1)) \quad w(z = 1) < -1. \quad (9)$$

This parametrization reproduces the behaviour of the growth factor to within 0.1%-0.5% accuracy for a wide variety of dark energy cosmologies (Linder 2005, Linder and Cahn 2007) and allows for a rapid scanning of

4

the parameter space of DDE models. We normalize the growth factors of the DE models to their high redshift behaviour ($D=\delta(a)/\delta(a=0)$) corresponding to WMAP normalization of the matter power spectrum. This procedure yields slightly different values of σ_8, the power spectrum normalization in terms of the variance of the density field smoothed over regions of 8 h^{-1} Mpc for different DE models. For the ΛCDM cosmology this corresponds to $\sigma_8 = 0.8$ for the local ($z = 0$) variance of the density field (Planck collaboration 2018); such a value vary by less than 2 % when different combinations (w_0, w_a) are assumed.

Both the distance relation (eq. 6) and the growth factors (eq. 8) of DDE models deviate mildly from the cosmological constant case when the equation of state is negatively evolving with redshift w_a <0, while models with w_a >0 yield growth factors and cosmic times lower than those predicted in the ΛCDM case. This is because in the w_a >0 models the influence of DE at early times is strong even at high redshift (see eq. (5)), yielding shorter ages and implying a delay in the growth of DM perturbations compared to the ΛCDM case (see fig. 1 in Lamastra et al. 2012).
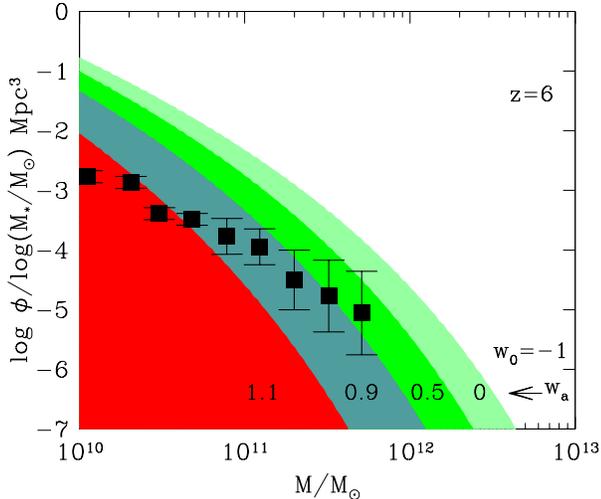
Fig. 1. The halo mass function at $z = 6$ predicted by different DDE models with $w_0 = -1$ and $w_a = 0$, 0.5, 0.9, 1.1 (from right to left, light green, green, dark green, and red colors, respectively). The black dots correspond to stellar mass function measured by Grazian et al. (2015) at $z = 6$; for the sake of simplicity, in this plot a conversion factor $M_*/M = f_b$ has been assumed to assign a DM mass to the stellar mass of the measured data point.

The impact of the above effects on the predicted abundance of halos (eq. 1) is illustrated in fig. 1. We show the DM mass function derived from eq. (1) in selected DDE cases with four different values of w_a (0 , 0.5, 0.9, 1.1) and fixed $w_0 = -1$. For a prompt comparison, we have also shown the mass distribution of galaxies (with the $2 - \sigma$ errorbar) corresponding to the stellar mass function by Grazian et al. (2015), assuming that all baryons are converted into stars, i.e., $M_*/M = f_b$, to convert the observed stellar mass M_* to the halo DM mass M (see Sect. 3.1 for a detailed comparison).

While the mass function of observed galaxies is expected to be lower than the halo mass function due to the inefficient conversion of baryons into observable stellar mass, luminous galaxies cannot outnumber their host DM halos. Thus, the DM mass function in the figure should be considered as *upper limits* for the mass distribution of observed galaxies.

The rapid, exponential decline of the DM mass function at large masses (eqs. 1 and 2) results into a large sensitivity of the predicted abundance of massive DM halos on the growth factor $D(z)$ corresponding to the different considered DDE models. As a result, in DDE models with $w_0 = -1$ and $w_a \geq 1.1$ the maximal abundance of massive DM halos is too low (deviation larger than $2 - \sigma$) to account for the observed number density of massive galaxies.

The example above shows that selecting extremely massive objects at high redshift is essential to provide constraints on DDE models. Thus, in the following sections, we will compare DDE predictions with different observations concerning the most massive objects already in place at high redshifts.

3. Results

Here we compare the abundance of DM halos predicted by DDE models with different observations. When computing the mass function (eq. 1), we assume a matter density parameter $\Omega_M = 0.31$, a baryon density parameter $\Omega_b = 0.045$, corresponding to the values that provide the best fit to CMB data when w_0 and w_a are allowed to vary (see Di Valentino et al. 2017); similar results are obtained if we convolve our predictions with a Gaussian uncertainty distribution centered on the above values and with variance $\sigma_{\Omega_M} = 0.02$ and $\sigma_{\Omega_b} = 0.005$, respectively. For the Hubble constant we take the value $H_0 = 70$ km s^{-1} Mpc^{-1} although the best fit values to CMB (in combination with other probes) vary in the range $67 \leq H_0/$km s^{-1} Mpc$^{-1} \leq 74$ when w_0 and w_a are allowed to vary (Di Valentino 2017). In fact, the final constraints we obtain on the $w_0 - w_a$ plane

are weakly dependent on H_0 for the massive systems redshift range considered $z \approx 4 - 7$: for any given w_0, varying H_0 in the above range changes our constraints on w_a by less than 2%.

3.1. The Stellar Mass function at $z = 6$ from CANDELS

We first compare with the observed stellar mass distribution of massive, distant galaxies. Since stellar mass is a time-integrated quantity, it is less sensitive to the details of the star formation history and can be more easily related to the DM mass of the host halo. However, an extended wavelength coverage is essential for estimating stellar masses from SED (spectral energy distribution) fitting, while measuring the abundance of massive, rare galaxies requires a combination of survey volume and depth. The CANDELS project (Koekemoer et al. 2011; Grogin et al. 2011) takes advantage of the optical/near-infrared/mid-infrared imaging provided by Hubble Space Telescope (HST), Spitzer, and the Very Large Telescope, and provides an ideal data set to base on for such a measurement. Here we use the high redshift ($z = 5.5 - 6.5$) mass function derived by Grazian et al. (2015), who used a spectral-fitting technique to derive stellar masses for a galaxy sample with high-quality photometric redshifts based on the CANDELS-UDS, GOODS-South, and HUDF fields. To take into proper account the uncertainties related to the stellar mass measurements (in turn depending on age, dust extinction, metallicity, star formation history), and to photometric redshifts, star formation histories, cosmic variance and Poissonian statistical fluctuations, we have run a Monte Carlo simulation, specific to the adopted data set. This allows us to derive, for any chosen stellar mass bin, the whole probability distribution functions $p(\phi_{obs})$ (PDF hereafter) of measuring an abundance ϕ_{obs}.

We associate the stellar mass M_* to the host halo DM mass M using the relation $M_* = F f_b M$, where F describes the efficiency of baryon conversion into stars. While $F = 1$ corresponds to the complete conversion, the different processes (gradual gas cooling gas ejection, stellar feedback) taking place in galaxies limit F to lower values. In fact, the standard conversion for ΛCDM derived from abundance matching techniques (see, e.g., Berhhozi et al. 2018) yields values $F \approx 0.25$. Such a value cannot be safely considered as a baseline for generic DDE models, since the stellar masses derived from abundance matching assume a ΛCDM halo mass function. However, we can study the effectiveness of baryon conversion into stars using hydrodynamical N-Body simulations, since the physics of such a conversion is expected to weakly depend on the background cosmology. To this aim we analyzed the public release of three simulations: the Illustris simulations (Springel, 2010; Genel et al., 2014; Vogelsberger et al., 2014a,b), its updated version (IllustrisTNG, Weinberger et al. 2017; Pillepich et al. 2018), and the EAGLE simulation (Schaye 2015). For Illustris TNG we considered the highest resolution version of the largest and medium volume realizations (TNG300 and TNG100). We computed the conversion efficiency $F = (M_*/M)/f_b$ from the ratio between the DM mass M of each sub-halo in the simulations and the stellar content M_* associated to the considered sub-halo, finding that $F = 0.5$ constitutes an effective, conservative upper limit for such a quantity, since (in all simulations) no massive ($M_* \geq 3 \cdot 10^{10} M_\odot$) galaxies have been found with $F \geq 0.5$ at $z = 5.5 - 6.5$.

Then, we consider a grid of DDE models characterized by different combinations (w_0, w_a). For each combination (w_0, w_a) we first correct the observed abundances ϕ_{obs} with the volume factor $f_{Vol} = V_\Lambda/V_{w_0,w_a}$ (computed in the redshift range $z = 5.5 - 6.5$) to account for the fact that the mass function given in Grazian et al. (2015) have been derived assuming a ΛCDM cosmology. Analogously, we must take into account that the stellar masses measured by Grazian et al. (2015) have been inferred from luminosities assuming a ΛCDM cosmology to convert observed fluxes into luminosities. Thus, for each combination (w_0, w_a) we must correct the masses M_* measured by Grazian et al. (2015) by a factor $f_{lum} = D^2_{L,w_0,w_1}/D^2_{L,\Lambda}$ where D^2_{L,w_0,w_1} is the luminosity distance computed (at the considered redshift $z = 6$) for considered (w_0, w_a) combination, and $D^2_{L,\Lambda}$ is its value in the ΛCDM case.

We focus on the largest stellar mass bin (centered on $M_* = 8 \cdot 10^{10} M_\odot$ assuming a Salpeter IMF) analyzed by Grazian et al. (2015). For each combination (w_0, w_a) we compare the volume-corrected, observed abundance of galaxies $\tilde{\phi} = \phi_{obs} f_{Vol}$ with stellar mass $M_* = 8 f_{lum} 10^{10} M_\odot$ at $z = 6$ with the predicted number density $\phi_{w_0,w_a}(M)$ (eq. 1) of DM halos with DM masses larger than $M = M_*/(F f_b)$ for the considered (w_0, w_a) combination. The confidence for the exclusion P_{excl} of each considered DDE model is obtained from the PDF as the probability that the measured abundance is larger than number density predicted by the model, i.e., $P_{exl}(w_0, w_a) = \int_{\phi_{w_0,w_a}}^{\infty} p(\tilde{\phi}) \, d\tilde{\phi}$.

We show in fig. 2 the region of the $w_0 - w_a$ excluded at 2-σ confidence level (i.e., $P_{exl} \geq 0.95$) for $F = 1$, $F = 0.5$ and the $F = 0.25$ case. The exclusion region is overplotted to the regions allowed by CMB and weak lensing, and to the region derived by the combination of the same data with the Hubble diagram of supernovae and quasars (Risaliti and Lusso 2019). Our probe significantly restricts the region in DDE parameter space allowed by other methods. In particular, we exclude an appreciable part of the region favored by the distant quasar method.
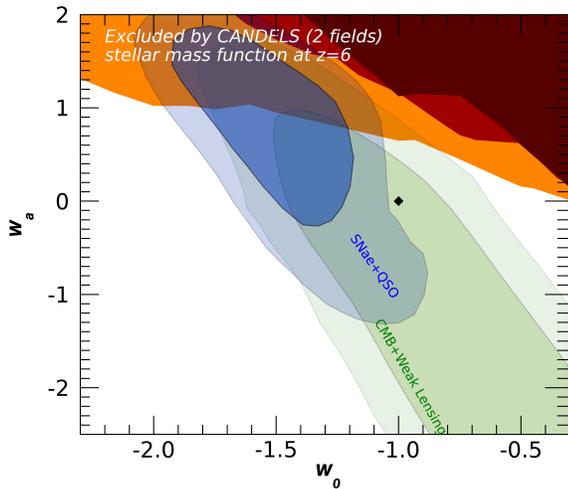
Fig. 2. Exclusion regions (2-σ confidence level) in the $w_0 - w_a$ plane derived from the observed CANDELS stellar mass function at $z = 6$ (Grazian et al. 2015). The brown, red, and orange regions correspond to assuming $F = 1$, $F = 0.5$, and $F = 0.25$, respectively (see text). Our **exclusion** region is compared with the $2 - \sigma$ and $3 - \sigma$ contours **allowed** by CMB+weak lensing (green regions) and by the combination of the same data with the Hubble diagram of supernovae and quasars (blue region), derived from fig. 4 of Risaliti and Lusso (2019). The black dot corresponds to the ΛCDM case ($w_0 = -1$, $w_a = 0$).

We stress that our method allows for significant improvements when more extended databases will be available in the future. To stress this point, we show in fig. 3 the constraints that would be obtained from the Grazian et al. (2015) stellar mass function if we decrease by 1/2 the dispersion in the PDF around the average value. This (approximatively) simulates the effects of the larger statistics that would be obtained analyzing the full CANDELS dataset (5 fields). In this case, most of the region allowed by distant quasars would be excluded even in the conservative case $F = 0.5$.
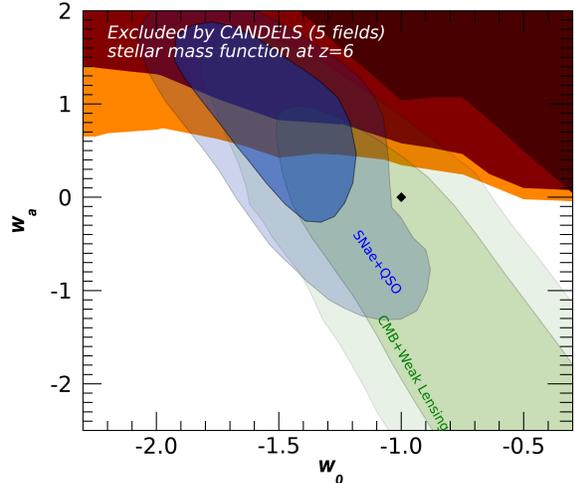
Fig. 3. As fig. 2, but assuming the errorbars of the stellar mass function reduced by 1/2, to simulate the inclusion of the full set of CANDELS field. This improvement would exclude most of the region allowed by distant quasars.

3.2. Massive galaxies detected in sub-mm at $z \approx 4$

The above population of galaxies (identified in rest-frame optical and ultraviolet) is known to under-represent the most massive galaxies, which have rich dust content and/or old stellar populations. These are however detectable at submillimetre wavelengths . Recently, Wang et al (2019) performed detailed submillimeter (870 micrometres) observations at the Atacama Large Millimeter Array (ALMA) of a sample of Spitzer/Infrared Array Camera (IRAC)-bright galaxies. They detected 39 star-forming objects at $z > 3$, which are unseen in even the deepest near-infrared (H-band) imaging with the Hubble Space Telescope (H-dropouts), which proved to be massive galaxies with median stellar mass extending up to $M_* \approx 3 \cdot 10^{11} \, M_\odot$, with a median mass $M_* \approx 4 \cdot 10^{10} \, M_\odot$.

For such objects we follow a procedure similar to what explained in the previous Section. We compute the number density of galaxies with stellar mass in the bin $10.25 \leq \log(M_*/M_\odot) \leq 10.75$ (dominating the statistics of observed objects) at redshifts $z = 4.5 - 5.5$, and derive the corresponding 2-σ lower limit $\phi_{low}(M_*) = 1.8 \cdot 10^{-5}$ Mpc^{-3}. To relate the observed stellar mass M_* to the DM mass M we adopt the highly conservative assumption $M = M_*/f_b$. We then computed the number density ϕ_{w_0,w_a} of DM halo mass corresponding to the observed M_* for different combinations (w_0, w_a), and compare it with the observed $2 - \sigma$ lower limit ϕ_{low}. For each combination (w_0, w_a), ob-

served number densities and stellar masses (measured assuming a ΛCDM cosmology) have been rescaled with the factors f_{Vol} and f_{lum} (see Sect. 2.1). The comparison allows us to exclude (at 2-σ confidence level) the combinations (w_0, w_a) for which $\phi_{w_0,w_a} < \phi_{low}$. The results is show as a brown exclusion region in fig. 4

Of course, the above approach is very conservative, since we assumed that the whole baryonic mass is in stars, and that the baryon mass of DM haloes is related to the DM mass through the universal baryon fraction (no loss of baryons). In fact, the very fact that the objects are characterized by a high star formation rate $\gtrsim 200\, M_*/$yr indicates that a sizable fraction of baryon is in the form of gas. Properly accounting for such gas fraction would yield larger values M associated to the observed M_* and - hence - tighter constraints. Although we have attempted to estimate the gas mass for the ALMA-detected H-dropout galaxies from the sub-mm continuum by converting the dust mass through the dust/gas ratio, the inferred gas masses are affected by large uncertainties (they span a range between $5 \cdot 10^9\, M_\odot$ and $5 \cdot 10^{10}\, M_\odot$), related to photometric redshifts (uncertainties are particularly critical given the steep shape of the spectrum in the far-IR), the adoption of a single and simplified gray body at the average temperature, and the adoption of the mass-metallicity at z=3.5 for all sources.
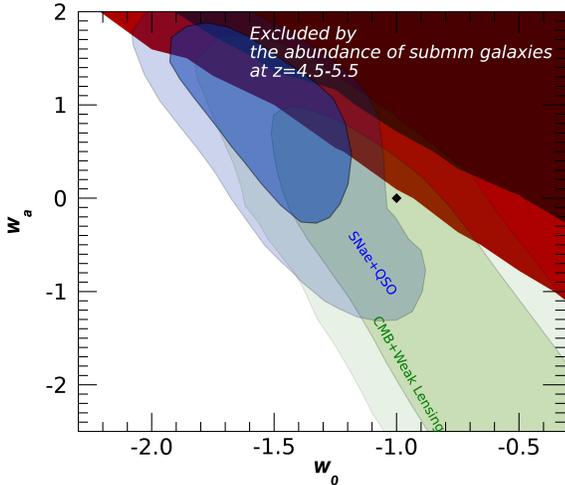
Fig. 4. Exclusion regions (2-σ confidence level) in the $w_0 - w_a$ plane (see text) derived from the observed abundance ϕ_{obs} of luminous submm galaxies at $z = 4.5 - 5.5$ (Wang et al. 2019). The brown region corresponds to assuming the observed stellar masses $M_* = M/f_b$ to be related to the DM mass through the baryon fraction f_b. The red regions corresponds to adopting the DM mass derived from the measured cross-correlation function of H-dropouts (see text).

To bypass the uncertainty related to the gas fraction, and to derive more realistic constraints for DDE models, we analyzed the clustering properties of the H-dropouts. We base on the procedure adopted by Wang et al. (2019) who estimated the two-point angular cross correlation function $\omega(\theta)$ of H-dropouts with all CANDELS galaxies in the redshift range $3.5 \leq z \leq 5.5$. Assuming a power-law form for the cross correlation $\omega(\theta) = A_\omega\, \theta^{-\beta} - IC$ (with $\beta = 0.8$ and IC the integral constraint in eq. 4 of Wang et al. 2019), the above authors derived the amplitude A_ω. This was related to the correlation length r_0 by the Limber equation (Croom and Shanks 1999; He, Akiyama, Bosch et al. 2018)

$$r_0 = \left[A_\omega\, \frac{c}{H_0\, Q}\, \frac{\int N_H(z)dz \int N_G(z)dz}{\int N_H(z)\, N_G(z)\chi^{1-\gamma}(z)\, E(z)dz} \right]^{1/\gamma} \quad (10)$$

where $\gamma = \beta + 1$, the constant $Q = \Gamma(1/2)\,\Gamma(\gamma/2 - 1/2)/\Gamma(\gamma/s)$ is a combination of Γ functions, $\chi(z)$ and $E(z)$ are given in eq. 5 and 6, and $N_H(z)$ and $N_G(z)$ are the redshift distributions of H-dropouts and CANDELS galaxies. The correlation length r_0 was then converted to galaxy bias through the relation (Peebles 1993)

$$b = \frac{72}{(3 - \gamma)(4 - \gamma)(6 - \gamma)2^\gamma\, \sigma_8(z)} \left[\frac{r_0}{8\, h^{-1}\mathrm{Mpc}} \right]^\gamma, \quad (11)$$

where $\sigma_8(z)$ is the amplitude of the dark matter fluctuation on the scale of $8\, h^{-1}$ Mpc. The DM mass is then derived from the relation $b = 1 + [\nu(M, z) - 1]/\delta_c$ (Mo and White 2002). For the standard ΛCDM case the above procedure yields $M = 10^{13\pm0.3}\, M_\odot$ for the average DM mass (Weng et al. 2019).

For our comparison with DDE predictions, we cannot take the above DM mass at face value, since it has been derived assuming a ΛCDM cosmology. In fact, for generic DDE cosmologies, the above value will (weakly) change due to two factors: i) the Limber equation (eq. 10) relating the observed A_ω to r_0 depends on cosmology through the functions $E(z)$ and $\chi(z)$ (Sect. 2) ; and ii) the different growth factor (Sect. 2, eq. 7 and below) affects the quantities $\nu(M, z)$ and $\sigma_8(z)$ entering the computation of the average mass M (eq. 11 and below). Thus, we computed the maximal effect of cosmology on the value of M derived by Wang et al. (2019) when our grid of values for the of combinations (w_0, w_a) is considered. Assuming the same measured angular cross correlation amplitude A_ω, we considered the effect of different cosmologies on the derived 3D correlation length

(eq. 10) and on the bias factor (eq. 11). We found that $M = 10^{13} M_\odot$ constitutes a (2-σ) lower limit for the value of the DM mass derived from cross correlation for any DDE model we considered. We then conservatively computed the DDE number density of objects with such a DM mass and compared it with the observed number density of H-dropouts with stellar mass $M_* = 10^{10.5} M_\odot$ (the average stellar mass of the sample). The resulting exclusion region in the (w_0, w_a) plane is shown in red in fig. 4.

3.3. SPT031158 at $z = 6.9$

The most massive system detected at $z \geq 6$ is a far-infrared-luminous object at redshift $z = 6.9$ originally identified in the 2500 deg^2 South Pole Telescope (SPT) survey (Marrone et al. 2018). Observation in the optical with the HST, infrared observations with the Spitzer Space Telescope, Gemini Optical/IR imaging and spectroscopy subsequently allowed for a characterization of this source. High-resolution imaging revealed this source (denominated SPT031158) to be a pair of extremely massive star-forming galaxies, with the larger galaxy (SPT031158W) forming stars at a rate of 2900 $M_\odot$/yr. An elongated faint object seen at optical and near-infrared wavelengths is consistent with a nearly edge-on spiral galaxy at $z \approx 1.4$ acting as a gravitational lens for the source, with an estimated magnification $\mu = 2$.

Measurements of the far-infrared continuum with the Atacama Large Millimeter/submillimeter Array (ALMA) led to estimate a huge H$_2$ gas mass $M_{H_2} \approx 3.1 \pm 1.9\, 10^{11} M_\odot$ for the whole system.

To estimate the DM mass associated to such object, we cannot follow the procedure adopted in Marrone et al. (2018), since they derive the gas-to-DM conversion factor from abundance matching techniques (see, e.g., Berhhozi et al. 2018) which cannot be safely considered as a baseline for generic DDE models, since they base on the ΛCDM halo mass function.

Thus, to estimate a conversion fraction from the observed H$_2$ mass to the DM mass we first adopt the conservative assumption that the total baryonic mass $M_b = M_* + M_{gas}$ (here M_{gas} is the total gas mass) is related to the DM mass through the baryon fraction $M = (M_* + M_{gas})/f_b$. Although no stellar light is convincingly seen from SPT031158W (probably due to the large extinction) a lower limit on the stellar content can be inferred from existing measurements of the molecular gas fration $f_{H_2} = M_{H_2}/(M_* + M_{H_2})$.

Measurements of high-z star forming galaxies (ranging from relatively quiescent BzK galaxies to dusty starbursts), suggest $f_{H_2} = 0.2 - 0.8$ (e.g. Daddi et al., 2010; Tacconi et al., 2010; Geach et al., 2011; Magdis et al., 2012; Combes et al., 2013; Tacconi et al., 2013, see Casey, Narayanan, Cooray 2014 for a review). However, all theoretical models (Benson et al. 2012; Lagos et al. 2012; Fu et al. 2012; Popping et al. 2014; Dave et al. 2012; see also Gabor and Bournaud 2013; Ginolfi et al. 2019) predict typically smaller values in the range $f_{H_2} \lesssim 0.5$. One possible solution to this mismatch has been offered by Narayanan et al. (2012), who suggested that the canonical conversion factor CO-H_2 was too large for the most extreme systems at high-redshift, and that the correct observed gas fractions are in the range $f_{H_2} = 0.1 - 0.4$. Similar conclusions are drawn by Tacconi et al. (2013) who suggested that the tension between galaxy gas fractions measured in observations and simulated galaxies may owe to incomplete sampling of galaxies.

Even assuming that H_2 constitute 80% of the gas mass (i.e., $f_g \equiv M_{H_2}/M_{gas} = 0.8$) at high redshifts (an upper limit according to Lagos et al. 2011, 2014) the estimated baryonic mass $M_b = M_{gas} + M_* = M_{H_2}(f_{H_2} + f_g - f_{H_2}f_g)/f_{H_2}f_g$ takes the value $M_b = 1.4\, M_{H_2}$ if we adopt the most conservative estimate $f_{H_2} = 0.8$, and $M_b = 2.75\, M_{H_2}$ if we adopt the estimate $f_{H_2} = 0.4$ suggested by theoretical models and by the effects suggested by Narayanan et al. (2012) or by Tacconi et al. (2013). This leads to associate to the observed M_{H_2} a DM mass $\overline{M} = M_b/f_b = 2 \cdot 10^{12} M_\odot$ in the most conservative case, and to $\overline{M} = M_b/f_b \approx 6 \cdot 10^{12} M_\odot$ in the other case; we will consider both values in the following analysis.

To estimate the rareness of such a system in all the considered DDE cosmologies, we compute the Poisson probability of finding such a massive object within the volume probed by the SPT survey, for different combinations (w_0, w_a). Following the method in Harrison and Hotchkiss (2013) as done in Marrone et al. (2018) for the ΛCDM cosmology, we first compute from eq. (3) the number $N(M, z)$ of systems with mass M and higher at redshift z and higher expected in the sky area f_{sky} covered by the SPT survey, for a grid of values of M and z. Then we compute such a number $N(\overline{M}, \overline{z})$ for the values $\overline{M}$ and $\overline{z}$ associated to the observed systems (i.e., $\overline{z} = 6.9$ and $\overline{M} = 2 - 6 \cdot 10^{12} M_\odot$ as discussed above). Finally, we consider the number N_{rare} defined as $N(M, z)$ computed only for the masses M and redshifts z for which $N(M, z) \geq N(\overline{M}, \overline{z})$, as dis-

cussed in Harrison and Hotchkiss (2013). The Poisson probability of observing at least one system with both greater mass and redshift than the one which has been observed is

$$R_{>\overline{M},>\overline{z}} = 1 - exp(-N_{rare}) \qquad (12)$$

The above probability depends on the region of the $M - z$ plane to which the SPT survey is sensitive (which provides the lower limit for the integration over redshift and mass in eq. 3), and on f_{sky}. Following Marrone et al. (2018) we assume that the survey is complete for $z \geq 1.5$ and for $M \geq 10^{11} M_{\odot}$, a conservative assumption as discussed in detail by the above authors. As for the effective fraction of the sky $f_{sky} = \Omega_{sky}/(41253 \text{ deg}^2)$ entering eq. 3, the total area corresponding to the SPT survey is $\Omega_{sky} = 2500 \text{ deg}^2$. However, Marrone et al. (2018) noticed that the effective survey area is potentially much smaller. In fact, most of the objects in the survey are strongly lensed, indicating that a source must be gravitationally lensed to exceed the 20mJy threshold for inclusion in redshift follow up observations. Given the uncertainties related to properly accounting for such an affect, we show our results for both the total area ($\Omega_{sky} = 2500 \text{ deg}^2$) and for an effective area reduced by 1/10 ($\Omega_{sky} = 250 \text{ deg}^2$) to illustrate the effect of such an uncertainty (Marrone et al. considered an even more extreme case $\Omega_{sky} = 25 \text{ deg}^2$).
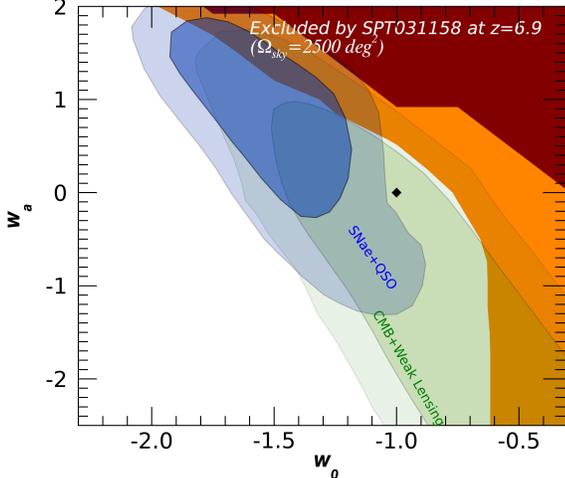
Fig. 5. Exclusion regions (2-σ confidence level) in the $w_0 - w_a$ plane (see text) for two different inferred DM mass of SPT031158: $2 \cdot 10^{12} M_{\odot}$ (red area) and $6 \cdot 10^{12} M_{\odot}$ (yellow area). In both cases the full SPT survey area $\Omega_{sky} = 2500 \text{ deg}^2$ has been assumed.

For each combination (w_0, w_a), we compute the expected number of systems like SPT031158 detectable

in the SPT survey. Then we associate a rareness to the resulting predicted number after eq. 10, and we compute the associated exclusion regions in the $w_0 - w_a$ plane. The result (2-σ confidence level) is shown in fig. 5 for the case $\Omega_{sky} = 2500 \text{ deg}^2$, for the two considered values $\overline{M} = 2 \cdot 10^{11} M_{\odot}$ (red region) and $\overline{M} = 6 \cdot 10^{11} M_{\odot}$ (orange region). In the latter case, corresponding to assuming the value $f_{H_2} = 0.4$ for the H_2 gas fraction, a major portion of the $w_0 - w_a$ is excluded, although the ΛCDM case ($w_0 = -1$, $w_a = 0$) remains allowed. The excluded region includes both the larger w_a cases allowed by the quasar method (blue region) and the cases $w_0 \geq -0.6$ allowed by the CMB+ weak lensing results, showing the potential impact of our results. Even tighter constraints are obtained for the case $\Omega_{sky} = 250 \text{ deg}^2$ shown in fig. 6.
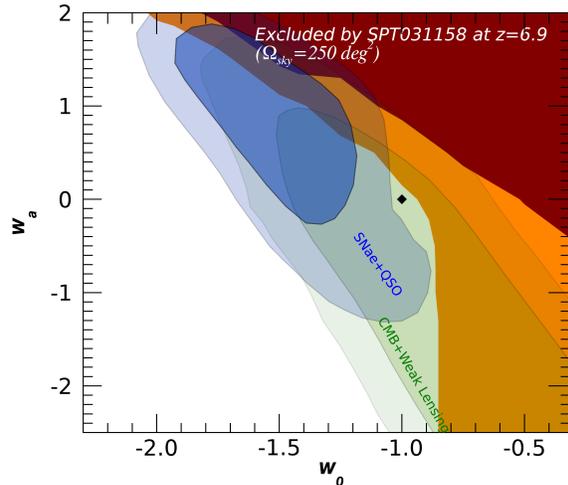
Fig. 6. Same as fig. 5, but assuming an affective SPT area $\Omega_{sky} = 250 \text{ deg}^2$.

3.4. Combining the different probes

In the previous sections (3.1-3.3) we have shown the potentiality of different observables as constraints on DDE models, and discussed how the effectiveness of each probe relies on how much the observed baryonic-to-DM mass ratio is suppressed with respect to the baryon fraction limit. While future observations will allow for a more precise determination of the gas and stellar mass fractions (see discussion in Sect.4 below), strong constraints can be derived - even under the most conservative assumptions - combining all the probes presented in Sect. 31.-3.3. In fact, the probabilities for each combination (w_0, w_a) to be consistent with each of the considered observations are independent. Thus we can derive a combined constraint by

multiplying the probabilities of being consistent with each probe. The resulting exclusion region is shown in fig. 7 adopting - for each probe in Sect. 3.1, 3.2 and 3.3 - the most conservative assumption for the relation between the observed baryonic component and the DM mass M: For the comparison with the CANDELS field we assume that the observed stellar mass is $M_* = 0.5 f_b M$ (i.e., $F = 0.5$, see Sect. 3.1); For the comparison with the abundance of submm galaxies (Sect. 3.1) we assume that the observed stellar mass is related to M by the baryonic fraction limit; As for the rareness of SPT031158, we take the conservative values for the gas mass fraction leading to a DM mass estimate $M = 2 \cdot 10^{12} M_\odot$ (see Sect. 3.3), and we consider the whole survey area ($\Omega_{sky} = 2500$ deg^2).

Inspection of fig. 7 shows that a major fraction of the parameter space favored by distant quasars combined with CMB and weak lensing is excluded at 2-σ confidence level, *independently on the details of the assumed baryon physics*.
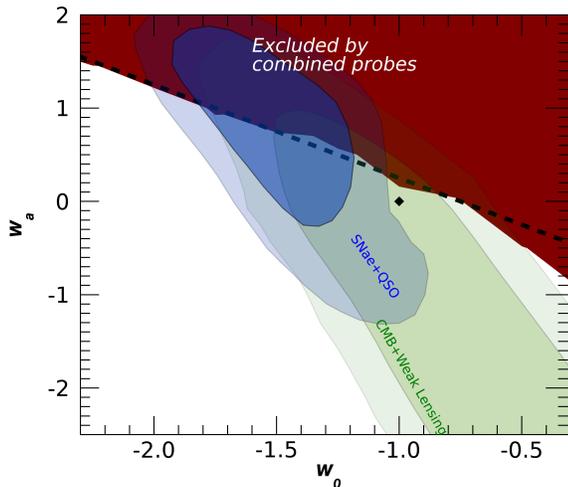
Fig. 7. Exclusion regions (2-σ confidence level) in the $w_0 - w_a$ plane derived from combining the different probes. For each observable, the most conservative case has been considered: for the CANDELS field we have assumed $F = 0.5$, for SPT031158 we have taken a DM mass $M = 2 \cdot 10^{12} M_\odot$, and for submm galaxies we have converted stellar masses to DM mass assuming $M = M_*/f_b$. The dashed line shows the analytical approximation for the boundary of the excluded region $w_a = -3/4 - (w_0 + 3/2)$.

4. Conclusions and Discussion

We have computed the abundance of massive systems predicted in different dynamical dark energy (DDE) models at high redshifts $z \approx 4-7$. Such predic-

tions have been compared with different observational probes: the bright end of the stellar mass function at $z \geq 6$, the space density of luminous submm galaxies at $z = 4 - 5$, and the rareness of the extreme hyperluminous infrared galaxy SPT031158 at $z \approx 7$.

We have derived exclusion regions in the parameter space $w_0 - w_a$ of DDE models from each of the above probes. Adopting the most conservative assumptions for the ratio between the observed baryonic component and the DM mass, we have combined the above results to derive conservative, robust constraints for the parameter space of DDE models, that do not depend on the details of the baryon physics involved in galaxy formation. In addition our results do not depend on the nature of the DM component, when present limits on the mass of DM particle candidates $m_X \gtrsim 3$ keV (see, e.g., Viel et al. 2013; Menci et al. 2016) are taken into account. In fact, for DM particle masses in the keV range (Warm Dark Matter) the associated power spectrum (Bode, Ostriker, Turok 2001; Destri, de Vega, Sanchez 2013) on the mass scales investigated in this work $M \geq 10^{10} M_\odot$ is identical to the CDM form assumed here, and our results are unchanged.

4.1. Implications of our Results

- When the most conservative values concerning the baryon-to-DM mass are assumed, our combined results allow to rule out DDE models with

$$w_a \geq -3/4 - (w_0 + 3/2)$$

  as displayed in fig.7, thus *excluding a major fraction* of the parameter space favored by the quasar distances (Risaliti and Lusso 2019), including the best-fit combination $w_0 \approx -0.8$ and $w_a = -1.5$ obtained with such a probe.

- Our results leave open the possibility that the present tension in the value of H_0 between the values derived from Planck and those obtained from local luminosity distance measurements be solved in DDE models, since the combinations (w_0, w_a) that allow to reconcile the different observations include values outside our exclusion region (see Di Valentino et al. 2017).

- On the other hand, our results *almost entirely rule out* the quintessence models where initially $w > -1$ and w decreases as the scalar rolls down the potential (cooling models), which occupy most of the region $w_0 > -1, w_a > 0$ (see Barger,

Guarnaccia , Marfatia 2005). These typically arise in models of dynamical supersymmtery breaking (Binetruy 1999; Masiero, Pietroni, Rosati 2000) and supergravity (Brax and Martin 1999; Copeland, Nunes, Rosati 2000) including the freezing models in Caldwell & Linder (2005) in which the potential has a minimum at $\phi = \infty$.

- For phantom models with $w_0 < -1$ (see Caldwell 2002), our constraint $w_a \geq -3/4 - (w_0 + 3/2)$ *excludes a major portion* of the parameter space corresponding to models for which the equation of state crossed the phantom divide line $w = -1$ from a higher value.

4.2. Improving constraints with improved measurements.

For each of the observables we considered, our constraints can be greatly tightened when improved, reliable measurements of the actual baryon fraction in galaxies, and of the relative weight of each baryonic component, will be available. E.g., a stellar to halo mass ratio $M_{star}/M = 0.25 f_b$ (a value favored by present hydrodynamical N-body simulations) would greatly tighten the constraints from the stellar mass function, allowing us to rule out all models with $w_a \geq 1$ presently allowed by the distant quasar method.

Also, the constraints from the abundance of submm galaxies at high redshifts could be greatly tightened when the gas mass of H-dropouts will be reliably measured. Spectroscopic follow-up of H-dropout galaxies with future facilities (e.g. the James Webb Space Telescope, JWST) will add a valuable improvement to the present analysis. Future measurements on the H_2 gas fraction at high redshift will also allow to reduce the present gap with respect to the theoretical expectations $f_{H_2} \approx 0.1 - 0.4$.

Observations of even a single infrared hyperluminous objects like SPT031158 at $z \approx 7$ would lead *to exclude all models with $w_0 \geq -0.6$, to ruling out a major fraction of the DDE parameter space presently favoured by CMB+weak lensing measurements.*

Such improved measurements will probably need the advent of future facilities. E.g., while a more accurate estimate of the gas-to-stellar mass fraction for the SPT031158 pair could in principle be inferred from

their stellar mass, the latter is currently poorly constrained: their rest-frame optical SED is only sampled by two (IRAC CH1 and CH2 for the Eastern source) and four (F125W, F160W, IRAC CH1 and CH2 for the Western source) photometric points, resulting into a $1 - \sigma$ uncertainty on the inferred stellar mass spanning a factor of $15 - 20$. In the next future, JWST will easily improve the accuracy in the stellar mass of the SPT031158 pair by providing a much more detailed characterization of the rest-frame optical and near-IR SED of these galaxies.

4.3. Statistics

Increasing the statistics of high-redshift massive objects will also greatly tighten present constraints (as shown by the comparison between figs. 2 and 3). Large surveys from space with the Euclid (Laureijs et al. 2011) and the Wide Field Infrared Survey Telescope (WFIRST, Spergel et al. 2015) satellites will increase the number of massive, high-z galaxies by orders of magnitude with respect to current HST samples. The Euclid surveys will cover 15000 deg^2 at $H \leq 24$ mag depth, and 40 deg^2 at $H \leq 26$, while the WFIRST High Latitude Survey will observe 2200 deg^2 at $H \leq 26.7$.

As a reference, the CANDELS GOODS-South sample comprises only one source with $M_{star} \approx 10^{11} M_\odot$ at $z \geq 6$ for $H \leq 24$, and 7 such sources at $H \leq 26.7$ on an area $\approx 0.05 \, deg^2$. The statistical uncertainty on the stellar mass function will thus be reduced by a factor $30 - 300$ by the aforementioned surveys, extending also to higher masses than those probed today. Unfortunately, systematic uncertainties will then dominate the error budget, mostly because the observed H band samples the rest-frame UV at $z \geq 6$ resulting in a potentially biased and incomplete selection of massive sources. In addition, the lack of information in the optical rest-frame adds significant uncertainties in the physical parameters estimated from SED-fitting. This problem will be overcome by JWST observations with the Mid-Infrared Instrument at $5.6 - 25 \mu m$, albeit on a much smaller area than Euclid and WFIRST.

Despite the lack of any plan for mid-IR large surveys from space, the combination of H-selected samples from future cosmological surveys, and improved characterization of high-z objects on smaller areas thanks to JWST, will lead to tighter constraints on the

high-mass end of the stellar mass function at $z \geq 6$, and thus on the parameter space (w_0, w_a) of DDE models.

REFERENCES

Achitouv, I.E., Corasaniti, P.S., 2012, JCAP, 02, 002

Ade, P.A.R., et al. (Planck Collaboration) 2016, A&A, 594, A14

Aghanim, N. et al. 2019, preprint (arXiv:1907.12875)

Addison, G.E., Huang, Y., Watts, D.J., et al. 2016, ApJ, 818, 132

Amara, A., Refregier, A. 2007, MNRAS, 381, 1018

Anderson, L., Aubourg, E., Bailey, S., et al. 2014, MNRAS, 441, 24

Barger, V., Guarnaccia, E., Marfatia, D. 2006, Physics Letters B 635, 61

Bardeen J. M., Bond J. R., Kaiser N., Szalay A. S., 1986, ApJ, 304, 15

Behroozi, P.S., Wechsler, R.H., Conroy, C. 2013, ApJ, 770, 57

Behroozi, P.S., Silk, J. 2015, ApJ, 799, 32

Behroozi, P.S., Silk, J. 2018, MNRAS, 477, 5382

Benson, A. J. 2012, New Astronomy, 17, 175

Beutler, F., Blake, C., Colless, M., et al. 2011, MNRAS, 416, 3017

Binetruy, P. 1999, Phys. Rev. D 60, 063502

Bode, P., Ostriker, J.P., Turok, N. 2001, ApJ, 556, 93

Bond, J. R., Cole, S., Efstathiou, G., Kaiser, N. 1991, ApJ, 379, 440

Brax, P., Martin, J. 1999, Phys. Lett. B 468, 40

Caldwell R.R. 2002, Phys. Lett. B 545, 23

Caldwell R.R., Dave R., Steinhardt P.J., 1998, Phys. Rev. Lett. 80 1582

Caldwell, R.R., Linder, E.V., 2005, Phys. Rev. Lett. 95, 141301

Caputi, K. I., Ilbert, O., Laigle, C., et al. 2015, ApJ, 810, 73

Carrol S.M., Press W.H., Turner E.L., 1992, ARA&A, 30, 499

Casey, C.M., Narayanan, D., Cooray, A. 2014, Physics Reports, Volume 541, Issue 2, 45

Chevallier M., Polarski D., 2001, Int. J. Mod. Phys. D 10,213

Chiba, T. 2006 Phys. Rev. D73, 063501

Chiba, T. 2009, Phys. Rev. D79, 083517

Combes, F., Garcia-Burillo, S., Braine, J., et al. 2013, A&A, 550, A41

Copeland, E.J., Nunes, N.J., Rosati, F. 2000, Phys. Rev. D 62, 123503,

Copeland E.J., Sahni M., Tsujikawa S., 2006, Int. J. Mod. Phys., D15, 1753

Corasaniti, P.S., Achitouv, I.E., 2011a, Phys. Rev. D, 84, 023009

Corasaniti, P.S., Achitouv, I.E., 2011b, Phys. Rev. Lett., 106, 241302

Croom, S.M., Shanks, T. 1999, 303, 411

Daddi, E., Bournaud, F., Walter, F., et al. 2010, ApJ, 713, 686

Dave, R., Finlator, K., Oppenheimer, B.D. 2012, MNRAS, 421, 98

Despali, G., Giocoli, R.E., Angulo, R.E., Tormen, G., Sheth, R., Baso, G., Mosacardini, L. 2016, MNRAS, 456, 2486

Destri, C., de Vega, P., Sanchez, N.G. 2013, Phys.Rev.D, 88, 3512

Di Valentino, E., Melchiorri, A., Linder, E.V., Silk, J. 2017, Phys. Rev., 100, 103520

Finkelstein, S. L., Song, M., Behroozi, P., et al. 2015, ApJ, 814, 95

Frieman J.A., Turner S., Huterer, D., 2008, ARA&A, 46, 385

Fu, J., Kauffmann, G., Li, C., Guo, Q. 2012, MNRAS, 424, 2701

Gabor, J. M., Bournaud, F. 2013, MNRAS, 434, 606

Geach, J. E., Smail, I., Moran, S. M.et al. 2011, ApJ, 730, L19

Genel S., et al., 2014, Monthly Notices of the Royal Astronomical Society, 445, 175

Ginolfi,M., Schneider, R., Valiante, R., MNRAS 483, 1256

Girelli, G., Bolzonella, M., Cimatti, A. 2019, A&A, 632, 80

Grazian, A., Fontana, A., Santini, p. et al. 2015, A&A, 575, 96

Grogin, N. A., Kocevski, D. D., Faber, S. M., et al. 2011, ApJS, 197, 35

Gupta, G., Rangarajan, R., Sen, A.A., 2015 Phys. Rev. D92, 123003

Harrison, I., Hotchkiss, S. 2013, J. Cosmology Astropart. Phys. 7, 022

He, W., Akiyana, M., Bosch, J. et al. 2018, Publ. Astron. Soc. Japan, 70 (SP1), S33

Heymans, C. et al., 2012, MNRAS, 427, 146)

Hildebrandt, H., Pielorz, J., Erben, T., et al. 2009, A&A, 498, 725

Hildebrandt, H. et al. 2017, MNRAS, 471, 4412

Hlozek R., et al., 2012, ApJ, 749, 90

Jenkins, A., Frenk, C.S., White, S.D.M., Colberg, J.M., Cole, S., Evrard, A.E., Couchman, H.M.P., Yoshida, N. 2001, MNRAS, 321, 372

Koekemoer, A.M., Faber, S.M., Ferguson, H.C., et al. 2011, ApJS, 197, 36

Lagos, C.d.P., Baugh C.M., Lacey C.G., Benson A.J., Kim, H.-S., Power C., 2011, MNRAS, 418, 1649

Lagos, C.d.P., Bayet, E., Baugh, C.M., Lacey, C.G., Bell, T.A., Fanidakis, N., Geach, J. E. 2012, MNRAS, 426, 2142

Lagos, C.d.P., Baugh, C.M., Zwaan, M.A., et al. 2014, MNRAS, 440, 920

Lamastra A., Menci N., Fiore F., Di Porto C. Amendola L. 2012, MNRAS, 420, 2429

Laureijs, R., et al., 2011, arXiv e-prints, arXiv:1110.3193

Lee, K.-S., Ferguson, H. C., Wiklind, T., et al. 2012, ApJ, 752, 66

Linder, E.V., 2003, Phys. Rev. Lett. 90 091301

Linder E.V., 2005, Phys. Rev. D, 72, 043529

Linder E.V., 2006, Phys. Rev. D, 73, 063010

Linder E.V., Cahn R. N., 2007, Astropart. Phys., 28, 481

Magdis, G. E., Daddi, E., Sargent, M. et al. 2012, ApJ, 758, L9

Maggiore, M., Riotto, A. 2010, ApJ, 717, 515

Mainini, R., Maccio, A.V., Bonometto, S.A., Klypin, A. 2003, ApJ, 599, 24

Marrone D.P., et al., 2018, Nature, 553, 51

Masiero, A., Pietroni, M., Rosati, F. 2000, Phys. Rev. D 61, 023504

Mehrabi, A. 2018, Phys. Rev. D, 97, 083522

Massey, R., Rhodes, J., Leauthard, A. et al. 2007, ApJS, 172, 239

Menci, N., Grazian, A., Castellano, M., Sanchez, N. G. 2016, ApJ, 825, L1

Merlin, E., Fortuni, F., Torelli, M. et al. 2019, MNRAS, 490, 3309

Mo, H.J., White, S.D.M. 2002, MNRAS, 336, 112

Moster, B.P., Naab, T., White, S.D.M. 2018, 477, 1822

Narayanan, D., Bothwell, M., Dave, R. 2012, MNRAS, 426, 1178

Pace, F., Waizmann, J.-C., Bartelmann, M. 2010, MNRAS, 406, 1865

Pan, S, Yang, W., Di Valentino, E., Saridakis, E.N., Chakraborty, S. 2019, Phys. Rev., 96, 023523

Peebles, P. J. E., Ratra B., 1988, ApJ, 325, L17

Peebles, P. J. E. 1993, Principles of Physical Cosmology (Princeton Univ. Press)

14

Pillepich A. et al., 2018a, MNRAS, 473, 4077

Popping, G., Somerville, R.S., Trager, S.C. 2014, MN-RAS, 442, 2398

Press, W.H., Schechter, P. 1974, ApJ, 187, 425

Refregier, A. 2003, ARAA, 41, 645

Riess, A. G., Macri, L. M., Hoffmann, S.L., et al. 2016, ApJ, 826, 56

Risaliti, G., Lusso, E. 2019, Nature Astron., 3, 272

Ross, A. J., Samushia, L., Howlett, C., et al. 2015, MNRAS, 449, 835

Sahlen, M., Liddle, A.R., Parkinson,D., 2007 Phys. Rev. D75, 023502

Sahni V., Wang L.M., 2000, Phys. Rev. D, 62, 103517

Schaye, J.,Crain, R.A., Bower, R.G. et al. 2015, MN-RAS, 446, 521

Scherrer, R.J. 2006, Phys. Rev. D73, 043502

Scherrer, R.J., Sen, A.A. 2008, Phys. Rev. D77, 08351515

Scolnic, D.M., Jones, D.O., Rest, A. 2018, ApJ, 859, 101

Sheth, R.K., and Tormen, G. 1999, MNRAS, 308, 119

Sheth, R.K., Mo, H.J., Tormen, G. 2001, MNRAS, 323, 1

Spergel, D., Gehrels, N., Baltay, C., et al. 2015, e-print, arXiv:1503.03757

Springel V., 2010, Monthly Notices of the Royal Astronomical Society, 401, 791

Sun G., Furlanetto S. R., 2016, MNRAS, 460, 417

Tacconi, L. J., Genzel, R., Neri, R. et al. 2010, Nature, 463, 781

Tacconi, L. J., Neri, R., Genzel, R. et al. 2013, ApJ, 768, 74

Tegmark M., Zaldarriaga M., 2002, Physical Review D, 66, 103508

Tegmark M., Zaldarriaga M., 2009, Physical Review D, 79, 083530

Tinker J., Kravtsov A. V., Klypin A., Abazajian K., Warren M., Yepes G., Gottlo ber S., Holz D. E., 2008, ApJ, 688, 709

Viel M., Becker G. D., Bolton J. S., Haehnelt M. G. A., 2013, Phys. Rev. D, 88, 3502

Vogelsberger M. et al., 2014a, MNRAS, 444, 1518

Vogelsberger M. et al., 2014b, Nature, 509, 177

Wang, T., Schreiber, C., Elbaz, D. et al. 2019, Nature, 572, 211

Warren, M. S., Abazajian, K., Holz, D. E., Teodoro, L. 2006, ApJ, 646, 881

Weinberg S., 1972, Gravitation and Cosmolgy: Principles and Applications of the General Theory of Relativity, John Wiley and Sons, New York

Weinberger R. et al., 2017, MNRAS, 465, 3291

Zhai, Z., Blanton, M., Slosar, A., Tinker, J. 2017, MN-RAS, 850, 183